A numerical investigation of a turbocharger compressor back-disk cavity at widely varying operating conditions

Turbocharging Seminar 2018
16-17 October 2018, Shanghai, China

A NUMERICAL INVESTIGATION OF A TURBOCHARGER COMPRESSOR BACK-DISK CAVITY AT WIDELY VARYING OPERATING CONDITIONS

Lee Gibson[1], Stephen Spence[1], Sung In Kim[1], Martin Schwitzke[2], Andre Starke[2]
1. Queen's University Belfast, Belfast, United Kingdom
**Corresponding author. Tel.: +44 28 9097 4569, E-mail: lgibson17@qub.ac.uk*
2. IHI Charging Systems International GmbH, Heidelberg, Germany

Abstract

There is an ever-growing demand for automotive turbocharger compressors to deliver a high boost-pressure efficiently over a wide range of engine operating conditions. At low turbocharger speeds, the engine operating line is close to the surge limit of the compressor wherein upstream blockage, for example, could result in system surge. Therefore, sufficient surge margin is required to ensure stable operation. Currently, the most effective method in operating range extension is through the use of a ported shroud (or bleed slot) casing treatment. However, extension typically comes at the cost of stage efficiency due to the mixing of high and low momentum flow at the inducer inlet. In recent years, active systems such as the on/off vaned diffuser and the swing vane type variable geometry vaned diffuser have gained more attention in the automotive sector due to their potential in improving both performance and range with minimum efficiency penalty. As part of a study of an on/off vaned diffuser concept, a vaned diffuser was designed for a small automotive turbocharger centrifugal compressor with a vaneless diffuser at the engine low-end torque point. Single-passage CFD simulations with the impeller back-disk cavity included showed a not insignificant drop in stage performance when compared to those without the cavity, which in turn motivated this numerical investigation. This CFD study aims to identify the key aerodynamic mechanisms responsible for reduced stage performance when the back-disk cavity is included at widely varying operating conditions. The results showed that for overall stage performance predictions, it was not essential to include the back-disk cavity, however for detailed aerodynamic investigations, particularly with vaned diffuser included, it was worth careful consideration.

Keywords

Internal combustion engines, turbocharging, centrifugal compressor, vaned diffuser

Nomenclature

Symbol	Description	Units
AS	Vaned diffuser aspect ratio (b_4/W_4)	[-]
c	Absolute velocity	[m/s]
c_p	Diffuser pressure recovery $\left(=\frac{p_5-p_3}{p_{03}-p_3}\right)$	[-]
b_4	Diffuser passage height	[mm]
p_{01}	Stage inlet total pressure	[Pa]
r_4/r_2	Radial gap ratio between vaned diffuser leading edge and impeller trailing edge	[-]
T_{01}	Stage inlet total temperature	[K]
Tu_1	Turbulence intensity at inlet	[%]
w	Relative velocity	[m/s]
W_4	Vaned diffuser throat width	[mm]
U	Blade speed	[m/s]
Z_1	Number of impeller blades (main + splitter)	[-]
Z_2	Number of diffuser vanes	[-]
$\dot{m}$	Mass flow rate	[kg/s]
Π_{tt}	Total-to-total pressure ratio	[-]
y^+	Non-dimensional first cell height	[-]
Y_p	Stagnation pressure loss $\left(=\frac{p_{03}-p_{05}}{p_{03}-p_3}\right)$	[-]

Subscripts

Max	Maximum value for given parameter
tt	Total-to-total
0	Total (stagnation) property
1	Stage inlet
2	Impeller trailing edge
3	Rotor-stator interface
4	Vaned diffuser leading edge
5	Volute inlet

Abbreviations

CFD	Computational Fluid Dynamics
BDC	Back-disk cavity
C	Coarse grid density
F	Fine grid density
LET	Low-end torque
M	Medium grid density
MP	Mixing-plane
MT	Maximum torque
RANS	Reynolds Averaged Navier-Stokes
RP	Rated power

1. Introduction

Centrifugal compressors used in automotive turbocharger applications require a wide operating range with high efficiency. In recent times, stringent emissions targets have forced engine designers to utilize high rates of exhaust gas recirculation (EGR) to reduce NO_X emissions [1]. In a high-pressure (or short-loop) EGR system, this forces the compressor to operate closer to the surge line due to the reduced mass flow rate through the compressor. Moreover, the compressor must provide a greater boost pressure to achieve the same power output; this is particularly true at low engine speed and load where high rates of EGR are often used. Thus, the emphasis on improving compressor efficiency and stability at low engine speeds is becoming more prominent.

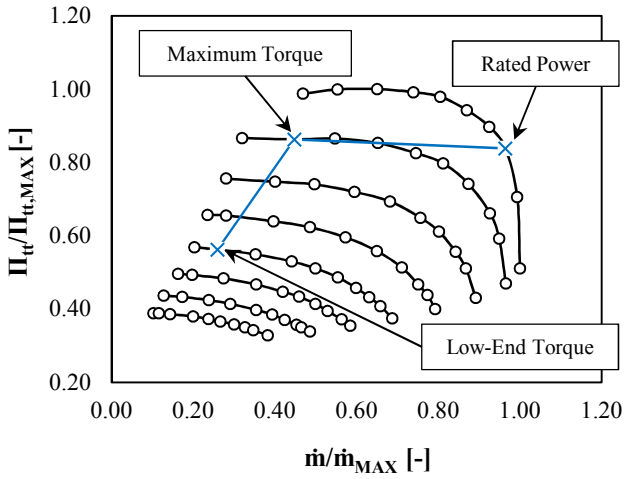

FIGURE 1: Experimental compressor map with engine full load line

Many methods exist for extending the stable operating range of centrifugal compressors. Passive methods such as axial casing grooves [2] and the ported shroud casing treatment [3] located in the inducer shroud region are proven to extend the operating range but at the cost of stage efficiency. Active systems such as the swing vane type variable geometry vaned diffuser have been investigated in the past and have shown great potential in maximizing the stable operating range with high efficiency [4, 5]. They are however, not typically utilized in passenger car turbochargers due to increased package size and cost. It is likely that future eBoosting concepts, where the compressor is driven by an electric motor, will be able to take advantage of active systems because of increased available space when the turbine is removed.

An active device which has received little attention is the so-called on/off vaned diffuser wherein a vaned diffuser is used at low engine speeds and flow rates and a vaneless diffuser at high engine speeds and flow rates. The primary role of the vaned diffuser is to improve stage efficiency near the surge line; Tange et al. [6] and Czapka et al. [7] reported some stability improvement using high and low solidity designs respectively. The vanes are then retracted where there is no longer a performance benefit and to ensure the choking flow rate of the stage is not reduced.

During the normal industrial design process of a vaned diffuser, and even in more detailed aerodynamics studies, the impeller back-disk cavity is often not included in CFD simulations due to the extra computational resources required such as the additional grid generation method and increased problem size. Based on existing reports in the open literature, the effect of back-disk cavity on stage performance and local flow aerodynamics is rather mixed.

Sun et al. [8] coupled their own back-disk cavity geometry, derived from a real centrifugal compressor, to that designed by Krain. For the case without leakage flows into or out of the cavity, as is often the case in turbochargers, a consistent reduction of around 0.5% in total-to-total isentropic efficiency was reported at 80-, 90- and 100% speeds from choke to surge. They highlighted that a low-pressure region behind the impeller trailing edge allowed high entropy flow leaving the back-disk cavity to mix with the coreflow and increase non-uniformity in this region.

Fischer et al. [9] investigated the effect of back-disk cavity geometry on stage performance and axial thrust load on the impeller using a full-stage CFD analysis of a turbocharger compressor with splitter blades. They reported the back-disk cavity had a negligible impact on stage pressure ratio predictions at low rotational speeds. At higher rotational speeds, however, the impact of the back-disk cavity on reducing the stage pressure ratio became more pronounced. The axial width of back-disk cavity between the impeller and bearing seal plate wall was found to influence the thrust loading on the wheel and power consumption. Specifically, a small axial width reduced the thrust loading on the compressor wheel but increased the power consumption where the opposite was true for an increase in axial width. However, the interaction between the cavity and impeller flows were not investigated in detail under different operating conditions.

Kaluza et al. [10] performed a high fidelity CFD analysis of a centrifugal compressor stage (single-bladed) with close-coupled pipe diffuser and exducer cavity. Within the cavity, flow was bled from the hub (aftbleed) and shroud (forebleed) in the vaneless space between the impeller and pipe diffuser. They identified a strong vortex (analogous to that found downstream of a backwards facing step) which was responsible for transporting flow in the circumferential direction and against impeller rotation direction in the trailing edge region. Near the trailing edge surface of the impeller, vortex breakdown was responsible for transporting fluid towards the shroud where it mixed with the coreflow thereby generating loss and reducing efficiency. Unfortunately, the flow structures in the impeller trailing edge region are only presented for a mid-speedline operating condition near peak efficiency of the compressor.

What is rather surprising is the limited information available with regards to the dominant flow mechanisms responsible for decreased performance in the impeller trailing edge region for a turbocharger compressor at widely varying operating conditions. Moreover, to the authors' knowledge, there are no studies published in the open literature considering the effect of back-disk cavity on vaned diffuser performance and

local flow aerodynamics. Information such as this could prove useful during the preliminary design process.

Paper overview: This paper aims to identify the key flow mechanisms responsible for reduced performance due to the back-disk cavity at low (and high) speeds and flow rates in a small turbocharger centrifugal compressor with splitter blades i.e. the engine low-end torque (LET) and rated power (RP) operating conditions; Figure 1.

2. Centrifugal Compressor Stage

The centrifugal compressor stage used in this work was of the standard automotive type consisting of an inlet nozzle, impeller with cut-off trailing edge(s), pinched vaneless diffuser and volute. No casing treatment or range extension device is used. Geometrical information of the compressor stage is contained in Table 1.

TABLE 1: Main compressor parameters

Parameter	Value	[Unit]
Impeller blade number Z_1	6 + 6	[-]
Diffuser vane number Z_2	17	[-]
Radial gap ratio r_4/r_2	1.10	[-]
Diffuser aspect ratio AS	0.85	[-]

2.1. Vaned Diffuser Design

It is well known that a centrifugal compressor with a vaned diffuser has a much narrower operating range than that with a vaneless diffuser. It is for this reason alone that they are not utilized in passenger car turbochargers. However, there are clear advantages in using a vaned diffuser such as improved efficiency and stability [11]. In this paper, a high-solidity design (small chord/pitch ratio) is preferred to a low-solidity design since only a small portion of the compressor map is required to be improved.

The high-solidity vaned diffuser shown in Figure 2 was aerodynamically designed at the LET operating condition using ANSYS BladeGen and CFX software. To minimize the wall-clock time per simulation during the design process, a single-passage of the stage axisymmetric components consisting of inlet pipe, impeller (without back-disk cavity and fillets) and vaned diffuser was defined. A key design parameter of a vaned diffuser is the aspect ratio (AS) of the throat. Runstadler et al. [12] found experimentally that the greatest pressure recovery was achieved with a value of unity (i.e. the throat width W_4 is equal to the passage height b_4) for a range of throat blockage and inlet Mach numbers. Clearly, this impacts the choking capacity of the stage, however in this application the objective is to improve efficiency near the surge line, therefore this is not deemed a critical factor. In this case, the number of diffuser vanes was chosen to provide an aspect ratio as close to unity as possible and also avoid a common multiple of the impeller blade count so as to try and minimize excitation during (future) experimental testing.

TABLE 2: Percentage change in performance using the vaned diffuser relative to the vaneless diffuser at LET

	$\Delta\eta_{01,05}$	$\Delta\eta_{01,5}$	Δc_p	ΔY_p
$\frac{\phi_{VD}-\phi_{VLD}}{\phi_{VLD}}$ (%)	2.01	9.85	50.62	-35.50

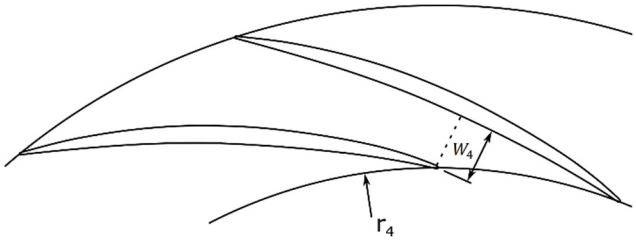

FIGURE 2: Curved camberline vaned diffuser

Ziegler et al. [13, 14] found experimentally that the radial gap between the diffuser leading edge and impeller trailing edge (r_4/r_2) can be sized to control the loading in the vaned diffuser, which is important with regards to pressure recovery and stability. Typically, this is chosen to ensure enough vaneless space diffusion of the flow to subsonic Mach numbers before reaching the diffuser leading edge [15]. For low to moderate pressure ratio stages (≤5), the best radial gap size is found to be in the region of 1.10 – 1.15 [16]. In this case a value of 1.10 was chosen as it was found to provide enough vaneless space mixing of the flow to provide relatively uniform (spanwise) incidence at the diffuser leading edge. Finally, the diffuser leading edge geometry was defined as having an elliptical ratio of 2:1. This "sharp" leading edge reduces flow deceleration around the leading edge of the vane and suppresses boundary layer development which is important for vaned diffuser stability [17].

2.1.1. Estimated Performance Improvements

With regards to performance evaluation, the primary evaluation planes of the stage are: (1) stage inlet, (2) impeller trailing edge, (3) rotor-stator interface, (4) vaned diffuser leading edge and, (5) volute inlet. A zero (0) before a particular location indicates a stagnation property was used in the calculation. For example, $\eta_{01,05}$ is the stage total-to-total efficiency evaluated between stage inlet and volute inlet.

Table 2 contains the estimated changes in performance using the designed vaned diffuser relative to the vaneless diffuser configuration; the computational set-up including solver details and boundary conditions is described in the forthcoming section. As expected, the vaned diffuser performs better than the vaneless diffuser at the LET operating condition. With regards to the diffuser stagnation pressure loss coefficient Y_p, the negative value indicates a reduction which is attritutable to the improved efficiency metrics of the stage. The primary advantage of the vaned diffuser configuration is that a rated boost pressure can be achieved at a lower turbocharger speed, thereby improving the engine transient response at low engine speeds. Specific engine improvements are not presented here and will form part of a future study.

TABLE 3: Percentage discrepancy between grids for a range of performance parameters at RP (vaneless diffuser configuration)

	$\Delta\eta_{01,05}$	$\Delta\eta_{01,5}$	$\Delta\Pi_{01,05}$	$\Delta\Pi_{01,5}$	$\Delta TR_{01,05}$	$\Delta\eta_{01,03}$	$\Delta\eta_{01,3}$	$\Delta\Pi_{01,03}$	Δc_p	ΔY_p
$\frac{\lvert\phi_C-\phi_M\rvert}{\phi_F}$ (%)	0.10	0.25	0.13	0.25	0.01	0.02	0.26	0.04	0.70	2.84
$\frac{\lvert\phi_M-\phi_F\rvert}{\phi_F}$ (%)	0.07	0.22	0.19	0.30	0.04	0.02	0.15	0.14	0.49	1.35

3. Numerical Method

3.1. CFD Model Configuration

The compressible 3D RANS equations were solved using the commercial ANSYS CFX 17.2 solver. The high-resolution advection scheme and turbulence numerics are employed. Turbulence was modelled using the SST turbulence model based on the findings of the previous study [18]. To allow accurate resolution into the boundary layer using the Low-Re formulation of the turbulence model, a $y^+ < 1$ was achieved throughout the majority of the domain. For vaneless diffuser simulations, the multiple reference frame (or Frozen Rotor) interface was defined between the rotating and stationary components. The mixing-plane interface was defined for simulations including the vaned diffuser to account for change in reference frame, pitch ratio and relative position of components. Solver convergence was deemed to be achieved whenever the RMS residuals fell below 1E-04, the mass, momentum and energy imbalances in each domain were less than ± 0.01% and the fluctuations in total-to-total efficiency were less than 0.05%.

Constant total inlet conditions of p_{01}= 100 kPa and T_{01}= 293.15 K along with a low turbulence intensity (Tu_1= 1%) was defined at compressor inlet. The latter value was chosen to simulate conditions within a settling chamber from which air is drawn into the compressor during (future) experimental testing. Each compressor operating condition was achieved by varying the mass flow rate at the outlet of the stage. The interface between the impeller and diffuser (vaned and vaneless) is $1.05r_2$ i.e. mid-way through the radial gap between the impeller and vaned diffuser. A summary of boundary conditions and interface locations is depicted in Figure 3.

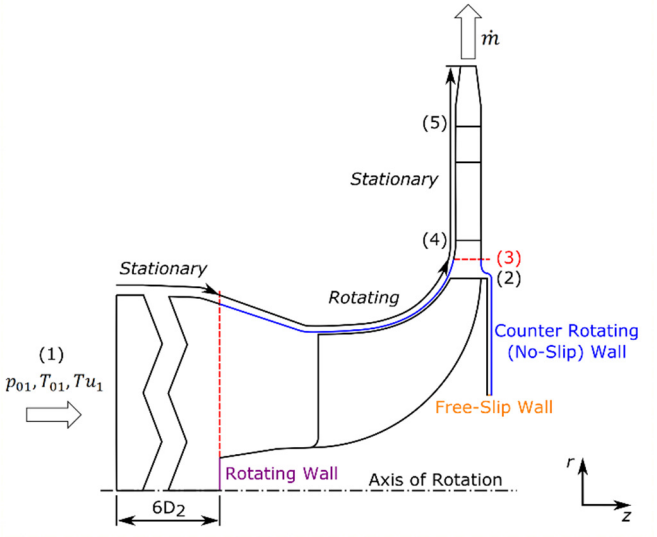

FIGURE 3: Meridional section of computational domain with interface locations and boundary conditions

3.2. Grid Convergence Analysis

Fully (structured) hexahedral grids of the inlet section, impeller with fillets and back-disk cavity, and vaneless diffuser were generated using ANSYS ICEM CFD. The vaned diffuser was meshed using ANSYS TurboGrid. Mesh quality targets of minimum orthogonality angle ≥23°, volume change ≤20 and aspect ratio ≤3000 have been met by all structured computational grids. To ensure the discretization error is low, a grid convergence analysis was performed at the three-engine related operating conditions depicted in Figure 1. Fine grids (F) for each component totaled approximately 5.5 Million cells in a single-passage of the stage i.e. inlet, impeller and back-disk cavity, and vaneless diffuser. The total number of cells in each component was then reduced by a factor of approximately 2 (twice) to generate the medium (M) and coarse (C) grids respectively. Solutions were found to be most sensitive to refinement at the RP operating condition and so only the results at this condition are presented. Percentage discrepancy between grids with regards to global and local performance parameters are presented in Table 3. Clearly the effect of refinement reduces the error between grids relative to the finest and that grid independence is being approached with the medium grid.

It is expected that the back-disk cavity will have a significant effect on the local flow aerodynamics in the impeller trailing edge region. For this reason, a separate sensitivity study was carried out using the medium grid. Figure 4 shows the effect of back-disk cavity refinement on the predicted circumferentially mass averaged total pressure distribution in the impeller trailing edge region. Approximately 0.5M cells are required to achieve grid independence in this area. A separate sensitivity study (not shown here) was also carried out for the number of cells in the blade tip gap. 25 cells were required to achieve grid independence in this case. The total number of cells making up a single-passage of the vaneless diffuser configuration is 3.7M. Finally, a separate grid convergence analysis was carried out for the vaned diffuser at an operating point close to choke at the maximum torque speedline using the inlet and impeller grids from the vaneless diffuser grid analysis. Approximately 0.6M cells were required to achieve grid independence for a single vaned diffuser passage at an operating condition close to choke at the maximum torque speedline.

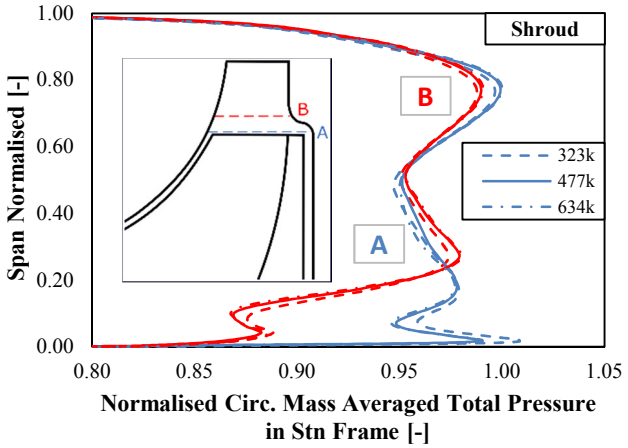

FIGURE 4: Circumferentially mass averaged total pressure distribution (hub to shroud)

4. Results

The effect of the back-disk cavity on performance is presented firstly for the vaneless and then for the vaned configuration.

4.1. Computational Method

To investigate the effect of the back-disk cavity on performance and local flow aerodynamics, two configurations were generated: one with, and another without the back-disk cavity. For the latter configuration, the mesh elements making up the cavity were not included in the simulation. This resulted in a slightly different hub-side contour in the impeller when compared to the conventional (or radially extended) method. However, the impact of this is expected to be negligible. Figure 5 shows a meridional section with the back-disk cavity removed and the aforementioned areas. With the back-disk cavity removed, the inlet surface is defined as a free-slip wall to prevent boundary layer growth. Rotor-stator interfaces defined for vaned and vaneless simulations are the same as those described in Section 3.1.

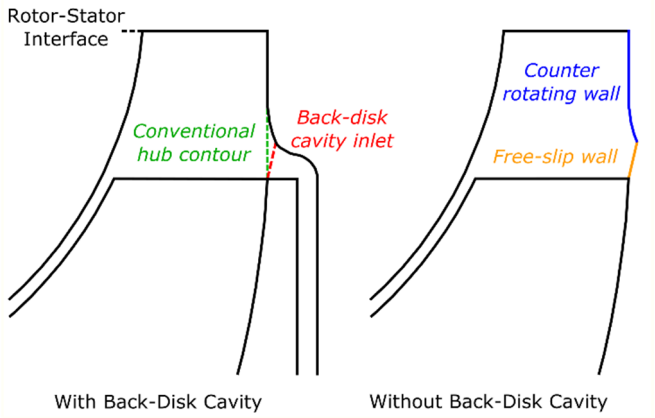

FIGURE 5: Meridional section of the computational domain with and without the back-disk cavity

4.2. Dominant Flow Features in the Impeller Trailing Edge Region Without the Back-Disk Cavity – Vaneless Configuration

Before investigating the effect of the back-disk cavity on performance, it is important to recognise the dominant flow structures present in its absence in the trailing edge region. To do so, single pitchwise planes are located at the impeller pressure side (Plane A) and suction side (Plane B) as shown in Figure 6; this is the location at which each contour plot in Figures 7 and 9 is shown. The same features are common to both the main and splitter blades albeit the former is greater in extent. For this reason, only results for the main blade are presented here.

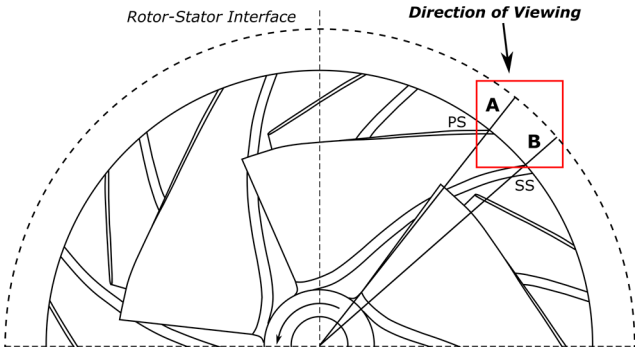

FIGURE 6: Impeller trailing edge pitchwise plane locations and direction of viewing

At the LET point there are strong secondary flow features present as shown in Figure 7 (a). At the shroud endwall ①, a region of self-contained recirculation exists which is brought about by excessive diffusion of the flow; some recirculation is also present at inlet to the vaneless diffuser on the hub side due to the thick impeller trailing edge wake ②. Near the hub pressure side corner of the blade, a small backwards facing step vortex is formed due to the sudden flow expansion over the blade fillet ③. This vortex grows from pressure side to suction side, as shown by the red arrow, along the trailing edge face of the blade by virtue of the pressure difference between channels. This results in the transportation of high entropy fluid downstream in the circumferential direction and against impeller rotation. Near the suction side of the blade ④, a region of recirculation extracts high entropy flow from the blade hub side wake and encourages mixing from hub to shroud. An acceleration of the mid-span flow occurs due to the blockage induced by this recirculation.

At the RP point similar flow structures are observed [Figure 7 (b)]. The shroud side recirculation reduces in size considerably ⑤ and the vaneless diffuser inlet recirculation disappears, as is to be expected when operating near choke at high speed. The suction side flow leaving the impeller is seen to deflect the vortex behind the trailing edge slightly further downstream ⑥. This results in a large mixing loss due to the interaction between the high entropy separated flow behind the trailing edge and the low entropy (transonic) flow leaving the impeller, as indicated by the steep relative Mach number gradient.

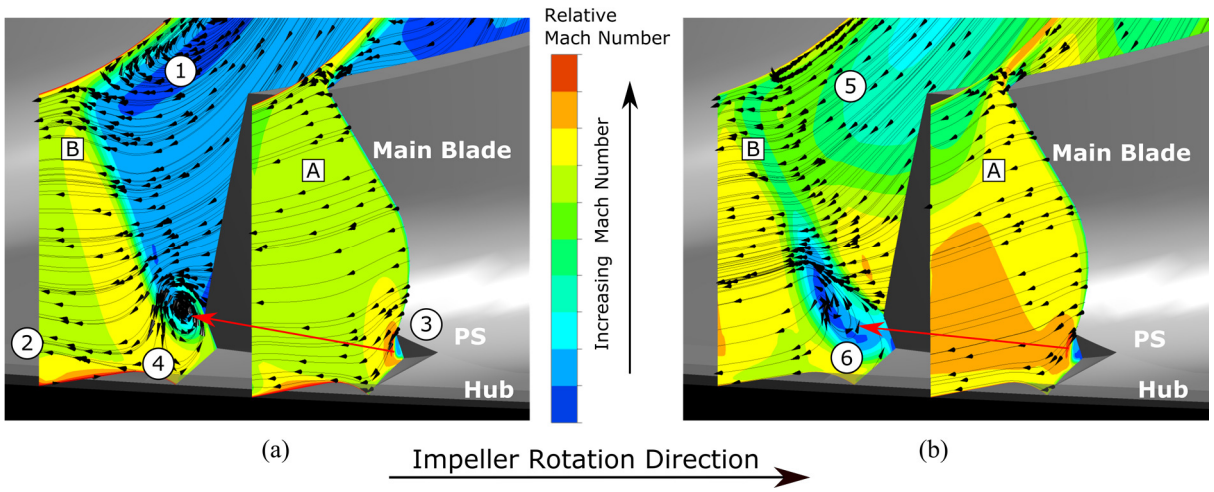

FIGURE 7: Secondary flow features behind the impeller main blade trailing edge without the back-disk cavity at (a) low-end torque and, (b) rated power operating conditions

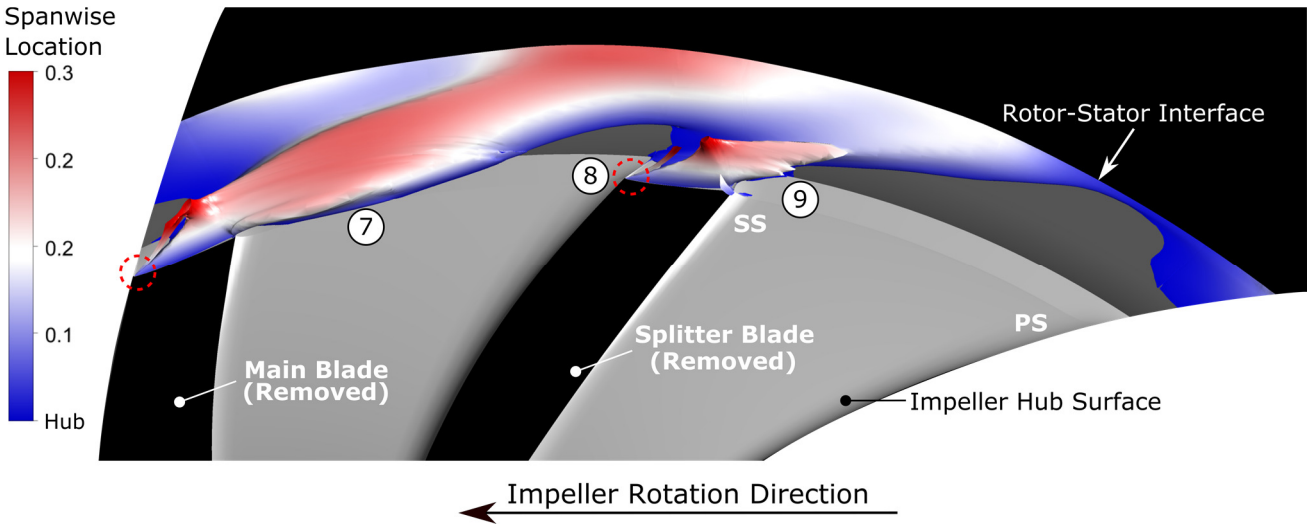

FIGURE 8: Isosurface of reversed streamwise velocity in the trailing edge region at the low-end torque operating condition. Each blade is removed to visualize the reversed flow behind each impeller blade trailing edge

4.2.1. 3D Visualisation of Reversed Flow in the Impeller Trailing Edge Region – Vaneless Configuration

To visualise the extent of flow separation in the trailing edge region, an isosurface of reversed streamwise velocity coloured by spanwise position is depicted in Figure 8 at the LET point; this isosurface is clipped to a maximum of 30% of the span for clarity. The point of flow separation that occurs at the pressure side corner of each blade is highlighted by the dashed red circles. Considering the main blade, this separation grows and interacts with the wake flow leaving the suction side of the main blade. As a result, a small amount of fluid, henceforth referred to as backflow, enters the compressor channel ⑦. This fluid is reworked by the impeller and mixes with the flow in the mid-span region. Moving towards the pressure side of the splitter blade, the reversed flow begins to decrease in size due to the relatively high momentum jet flow in this region ⑧. For the splitter blade, no backflow into the impeller occurs, due to an attached hub suction side boundary layer, and the region of reversed flow downstream of the trailing edge is smaller ⑨.

Before summarising the dominant flow features present in the trailing edge region without the back-disk cavity, it must be noted that the same impeller with fillets removed and a conventional hub side contour (Figure 5) did not show large separated regions behind the trailing edge nor in the downstream diffuser. Therefore, it is reasonable to assume that the extent of the pressure side hub separation at the trailing edge is primarily driven by the large fillet radius to impeller exit passage height ratio in this region (around half of the blade height). Unfortunately, this cannot be overcome in reality since the fillets are typically sized to reduce mechanical stresses in the compressor wheel.

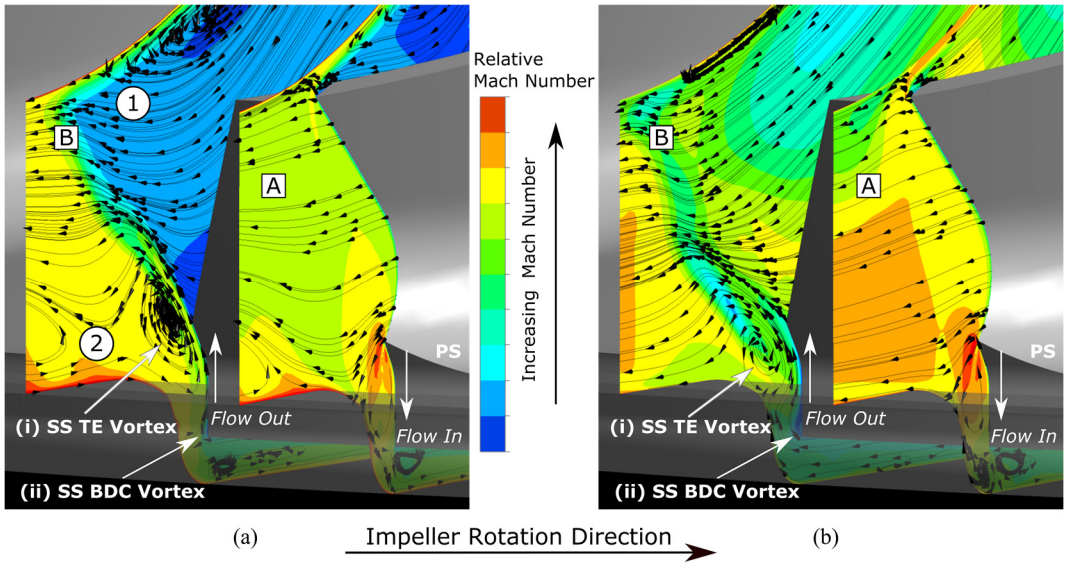

FIGURE 9: Secondary flow features behind the impeller main blade trailing edge with the back-disk cavity at (a) low-end torque and, (b) rated power operating conditions

Summary: At each operating condition considered it has been found that the flow separates from the pressure side blade fillet and forms a backwards facing step vortex. This vortex grows from pressure side to suction side along the trailing edge face due to the pressure difference between channels. At the suction side of the blade the interaction between the vortex and flow leaving the impeller depends on the operating condition. At low speeds and flow rates the vortex is part of a large recirculating zone of reversed flow. At high speeds and flow rates, the vortex size is reduced and is deflected slightly further downstream by the transonic flow leaving the impeller. In either case, this dominant flow structure acts to increase loss as shown by the steep Mach number gradient in Figure 7. With the dominant flow structures in the trailing edge region described, the back-disk cavity is now included in the computational model to determine its effect firstly on performance and then the local flow aerodynamics.

4.3. Effect of the Back-Disk Cavity on the Vaneless Diffuser Configuration

A number of conventional performance parameters have been chosen to quantify the effect of the back-disk cavity on both stage and component performance; Table 4. To avoid ambiguity, values are presented as percentage point differences between simulations with and without the back-disk cavity e.g. $\Delta\eta = \eta_{BDC} - \eta_{W/O\ BDC}$. Clearly, this often-disregarded component has a relatively large impact on stage performance predictions, the reasons for which will be described in the coming sections.

Before describing flow features exclusive to each operating condition responsible for this reduction in performance, there are some commonalities that must be highlighted first. The back-disk cavity itself acts as an inlet to the flow leaving the pressure side of each impeller channel as shown in Figure 9. Within the cavity, the flow significantly increases in temperature due to the high shear rate between the stationary bearing housing side wall and the rotating impeller. High pressure fluid then leaves the cavity by either (a) the depression directly behind the main or splitter blade trailing edges with high spanwise momentum as described by Sun et al. [8] or (b) the suction side of the channel by virtue of the existing pressure difference. Moreover, there exists two counter-rotating vortices in the suction side region: (i) the suction sided trailing edge vortex is formed due to the sudden flow expansion over the impeller blade pressure side fillet that spreads in the circumferential direction (as described in Section 4.2) and, (ii) the suction sided back-disk cavity vortex formed by the flow expansion over the sharp impeller shoulder within the cavity itself. The steep relative Mach number gradient in the suction side region implies high loss is incurred due to the interaction between these vortices. Similar flow features are observed at the pressure side, however, the loss incurred is significantly lower.

TABLE 4: Percentage point change in global and component performance with the back-disk cavity included

	$\Delta\eta_{01,05}$	$\Delta\eta_{01,5}$	$\Delta\eta_{01,03}$	$\Delta\eta_{01,3}$	Δc_p	ΔY_p
LET	-2.38	-2.42	-1.30	-1.75	-1.96	2.28
RP	-1.57	-2.54	-0.83	-0.95	-4.75	2.14

4.3.1. Low-End Torque (LET) Operating Condition

At the LET point with back-disk cavity included, the extent of reversed flow in the trailing edge region (and further downstream) is increased due to the interaction with the flow leaving the cavity near the suction side of the blade; Figure 9 (a). When compared to the case without back-disk cavity [Figure 7 (a)] the following changes to the flow in this region are found:

1. Acceleration of the coreflow due to an enlarged hub side blockage. A small reduction in recirculation at the shroud is also observed ①;

2. Increased vaneless diffuser hub-side recirculation and interaction with the backwards-facing step vortex caused by the blade fillet geometry ②;
3. Increased backflow into the impeller (not shown).

The first two points above result in a more radial flow angle at inlet to the vaneless diffuser and a reduced effective flow area. It is hypothesized that detailed design of the back-disk cavity could be used to exploit the hub side blockage near surge and help improve diffuser stability. On the other hand, the backflow into the impeller could be reduced by utilizing a hub-side vaneless diffuser pinch as described by Japikse [19]. However, the aforementioned concepts are beyond the scope of the present work but could form part of a future investigation. Finally, the effect of the backflow has a number of impacts on the impeller exit conditions and will be treated separately.

4.3.1.1 Effect of increased backflow on impeller outlet conditions

It has been shown that the inclusion of the back-disk cavity results in a strengthening of the secondary flow structures in the impeller trailing edge region. With regards to impeller backflow, the suction sided trailing edge vortex is found to be the dominant flow mechanism [Figure 9 (a)]. High loss flow extracted from the cavity is mixed in the spanwise direction with the impeller wake and the separated flow in the trailing edge region increases in size. An implicit result of this is a larger amount of backflow into the impeller.

To understand the effect of increased backflow, velocity triangles in the trailing edge region at the hub, mid-span and shroud are depicted in Figure 10. For this analysis a "Blade Aligned Turbo Surface" was defined near the impeller trailing edge. An Iso-Clip of this surface was used to distinguish between the active and recirculating flow regions as described by Harley et al. [20] and Stuart et al. [21]; in essence, the active flow region is assumed to contribute to the stage outflow conditions, whereas the recirculating flow region acts as a parasitic loss which results in an increase in stage total temperature rise and thus a reduction in efficiency. It must be noted that the additional region of backflow presents itself as a reversed flow region but is not self-contained as with inlet and trailing edge (shroud) recirculation.

According to the continuity equation at a given operating condition, the effect of increased blockage is expected to provide an acceleration of the meridional component of velocity. This results in less diffusion of the flow due to the increase in relative velocity and a lower static pressure rise across the impeller. When considering the velocity triangles along the span this is found to be the case. There are however some subtle changes in the mid-span and shroud regions. The backflow that leaves the back-disk cavity has a high relative swirl component. Upon entering the impeller channel, this backflow mixes with and diverts the coreflow in the mid-span region towards the pressure side of the splitter blade. Aside from increasing loss in this region, the meridional velocity is accelerated, and a small amount of relative swirl is added to the flow. Near the shroud, a *very small* increase in absolute swirl and therefore work input occurs due to a reduction in shroud side blockage as shown in Figure 10.

4.3.2. Rated Power Operating Condition

At high speeds and flow rates, no backflow into the impeller channel is predicted to occur without the back-disk cavity present. The reason for this is that the hub suction side boundary layer remains attached. This is to be expected since the flow has high momentum near choke at high speeds and is less likely to separate (in the absence of shocks). Upon introduction of the back-disk cavity however, backflow was found to occur but only into the suction side corner of each impeller blade (Figure 11). At the main blade, the flow traverses along the trailing edge towards the shroud up to the point of separation due to the spanwise adverse pressure gradient ①. This flow is then collected by the pressure side flow and mixed out downstream into the diffuser. A similar feature is found to occur in the splitter blade trailing edge region. However, the flow does not separate and instead interacts with the tip leakage flow ②. The reason for this is due to the shallower adverse pressure gradient at the splitter blade when compared to the main blade.

Interaction between the tip gap and backflow incurs a high mixing loss near the shroud which extends downstream into the vaneless diffuser. Inspection of the flow structures in the splitter blade tip gap region highlighted that the separation bubble increases in size. This is found to reduce the over- tip jet velocity which is known to be beneficial in removing low-energy flow from the shroud suction side corner. Although this is a subtle point, it must be emphasized that the dominant cause of reduced performance at this operating condition is the mixing of the high loss flow from the back-disk cavity

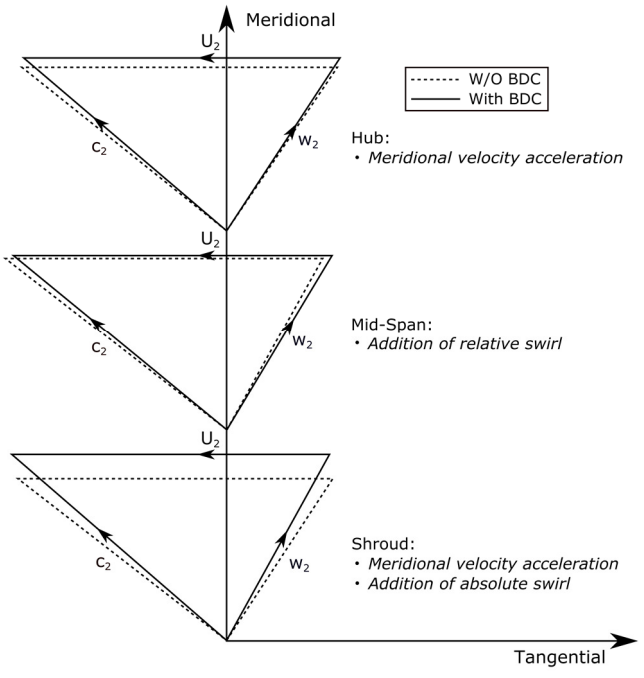

FIGURE 10: Effect of backflow on impeller trailing edge velocity triangles at low-end torque

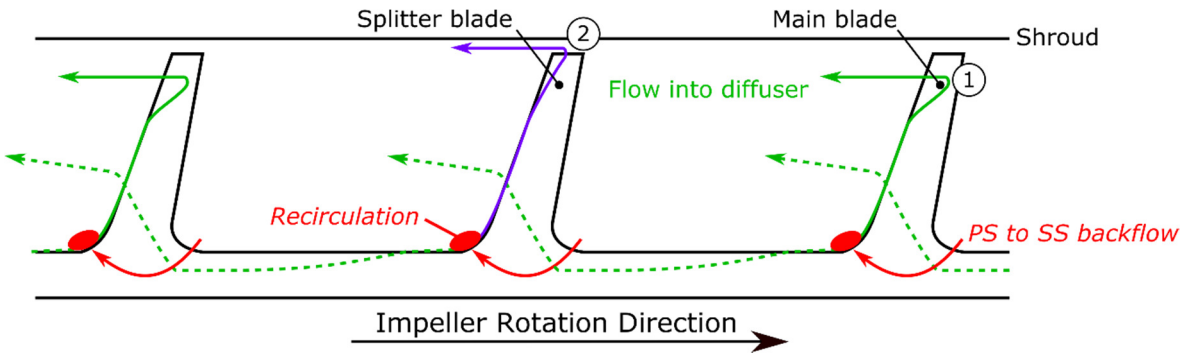

FIGURE 11: Dominant flow features in the impeller trailing edge region with the back-disk cavity included at the rated power operating condition

throughout the impeller trailing edge region and further downstream into the vaneless diffuser.

4.3.3. Effect on Vaneless Diffuser Performance

It is well-known that the flow entering the vaneless diffuser is highly non-uniform in both the spanwise and pitchwise directions, particularly near surge where the jet/wake flow structure typically dominates. Inclusion of the back-disk cavity further exacerbates non-uniformity due to mixing between the high entropy flow leaving the cavity near the blade suction side and the coreflow leaving the impeller (see Figure 9). As well as increasing loss, the back-disk cavity increases blockage that spreads into the vaneless diffuser, resulting in a more radial absolute flow angle. On the other hand, near choke the flow angle decreases slightly resulting in a longer flow path which is undesirable due to the associated pressure losses.

4.4. Effect of Back-Disk Cavity on Vaned Configuration

So far, the effect of the back-disk cavity on the vaneless diffuser configuration has been considered at both low and high speeds and flow rates. For the vaned configuration, only the LET operating condition is considered. However, before discussing the effect of the back-disk cavity on performance it is important to highlight, upon inclusion of the cavity, similar flow structures are predicted from the impeller trailing edge up to the rotor-stator interface between the vaned and vaneless configurations:

- Increased backflow from impeller pressure side to suction side which results in a small increase in stage total temperature rise (relative increase of around 0.2%);
- Increased hub-side reversed flow which blocks up to 30% of the span near the suction side channel of the main blade;
- Small reduction in shroud-side recirculation due to an acceleration of the coreflow around the hub-side blockage.

As described in Section 3.1, a mixing-plane interface is defined between the impeller and vaned diffuser. It is well known that this interface provides an unphysical circumferentially uniform velocity profile to the vaned diffuser. A recent study by the authors comparing the mixing-plane and transient blade-row Time Transformation methods yielded surprisingly similar results at the design point of the vaned diffuser i.e. the LET point. The primary difference between the two was that the loss was slightly under predicted by the mixing-plane method. This was because the unsteady mixing that occurs between the impeller trailing edge and diffuser leading edge was not being captured by the mixing-plane method. Besides, due to the much higher computational effort required by the transient method, steady-state CFD is deemed a reasonable compromise to study changes in the vaned diffuser flow field caused by the back-disk cavity.

4.4.1. Changes in Vaned Diffuser Leading Edge Incidence

It is well known that vaned diffuser performance and stability is heavily dependent on the quality of the flow exhausted from the impeller. A critical factor, particularly with regards to stability is incidence. In this paper, incidence is defined as the difference between the flow angle and blade metal angle at the diffuser leading edge. To extract this information, a Turbo Line was located just upstream of the leading edge and in-line with the blade metal angle. Figure 12 shows that the effect of the back-disk cavity on leading edge incidence is relatively small; the sub-diagram depicts the incidence convention employed. Upstream of the mixing-plane interface, a slightly more radial shroud side flow occurs due

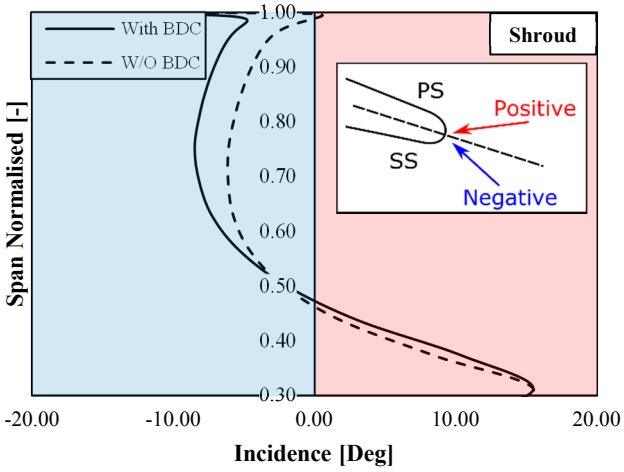

FIGURE 12: Incidence angle upstream of diffuser leading edge. Below approximately 30% span is blocked by reversed flow

to the increased blockage in the trailing edge region of the impeller. Just downstream of the mixing-plane the extent of the blockage remains similar. Based on these findings, it is reasonable to say that the presence of the back-disk cavity relative to the case without tends to move the vaned diffuser operating condition to a higher mass flow rate. This is useful from a design perspective since the vane setting angle (pivoted about the leading edge) could be set slightly more radial to achieve an incidence angle close to zero if this were the design target at low speeds and flow rates.

4.4.2. Effect of Increased Negative Incidence

To visualize the effect of increased negative incidence, a contour of "Momentum Density", which is defined as the product of local density and streamwise velocity, is depicted in Figure 13 at 75% diffuser span near the shroud; this is the location where the largest difference in incidence occurs between cases. At inlet to the vaned diffuser ①, the momentum of the flow is increased due to an acceleration of the coreflow by the presence of the hub-side blockage. This results in a more radial flow angle near the shroud (as shown in Figure 12) and thus acceleration around the leading edge of the diffuser vane ②. As a result of this, flow separation from the vane occurs at a streamwise location slightly further upstream ③. However, this does not impact diffuser performance significantly.

It must be emphasized that the primary mechanisms responsible for reduced performance is the increased backflow into the impeller and mixing of the cavity flow with the co

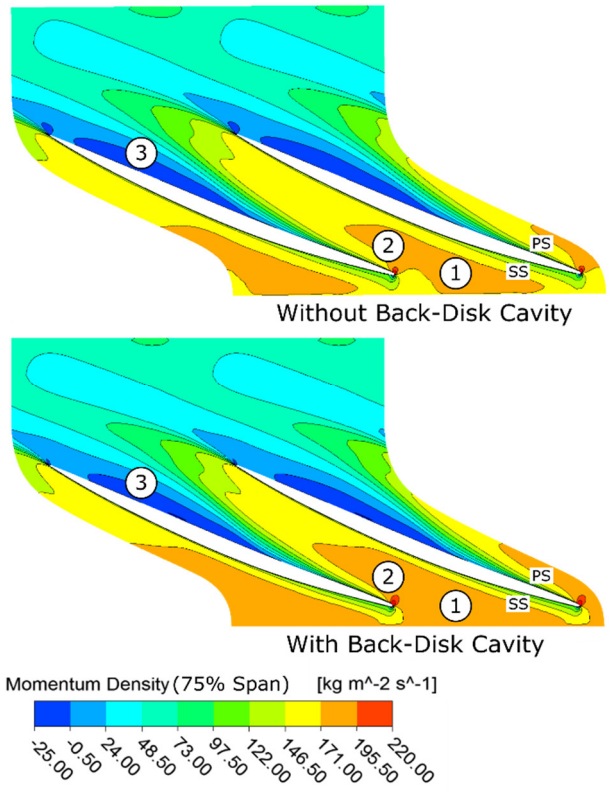

FIGURE 13: Contour of momentum density at 75% span in the vaned diffuser

reflow before entering the vaned diffuser. Future unsteady simulations will be used to study the interaction between the impeller, back-disk cavity and vaned diffuser. It is hoped that these findings will improve the understanding of the vaned diffuser flow field whenever the cavity is present and help guide design changes.

5. Conclusions

A numerical investigation carried out to determine the effect of the impeller back-disk cavity on performance and local flow aerodynamics in the impeller trailing edge region has been presented. It was found that at both engine related operating conditions (low-end torque and rated power) that the cavity permitted flow to enter (near the blade pressure side) and leave (near the blade suction side). At low-speeds and flow rates this resulted in a strengthening of the backflow into the impeller main blade suction side channel. This resulted in a slight increase in total temperature (up to 0.3% relative to the case without the back-disk cavity for the vaneless configuration) due to the additional work done on the flow by the impeller and an acceleration of the flow around the backflow region due to its inherent aerodynamic blockage effect. At high speeds and flow rates, the back-disk cavity flow entered the impeller suction side corner of each blade with high spanwise momentum. For the main blade, flow was found to mix out in the trailing edge region and travel downstream into the diffuser. In the case of the splitter blade however, some of the flow travelled into the tip gap and mixed with the tip leakage flow. Aside from increasing loss, this reduced tip leakage jet strength and increased blade loading near the shroud. Rather surprisingly, the cavity has a relatively minor influence on overall stage performance predictions at the design point of the vaned diffuser i.e. approximately 1% reduction in efficiency. A more radial flow from approximately 50% span upwards occurs due to the acceleration of the coreflow caused by the increase in blockage in the impeller trailing edge region. However, it can be expected that the influence of the cavity will become more significant at the upper speedlines, as highlighted by Fischer et al. [9]. With regards to geometrical influence on performance, it is believed that the inlet geometry of the back-disk cavity (i.e. the hub-side contour) is the main parameter driving the interaction.

Acknowledgements

The authors would like to sincerely thank IHI Charging Systems International GmbH for their technical and financial support. The authors would also like to extend their thanks to ANSYS Inc. for the use of their CFD software and their technical support during this programme of research.

References

[1] Arnold, S., 2008, "Single Sequential Turbocharger: A New Boosting Concept for Ultra-Low Emission Diesel Engines," SAE Int. J. Engines, **1**(1), pp. 232-239.

[2] Harley, P. X. L., Starke, A., Bamba, T., and Filsinger, D., 2017, "Axial Groove Casing Treatment in an Automotive Turbocharger Centrifugal Compressor," Proceedings of the Institution of Mechanical Engineers, Part C: Journal of Mechanical Engineering Science, pp. 1-13.

[3] Sivagnanasundaram, S., Spence, S., Early, J., and Nikpour, B., 2010, "An Investigation of Compressor Map Width Enhancement and the Inducer Flow Field using Various Configurations of Shroud Bleed Slot," ASME Turbo Expo 2010: Power for Land, Sea and Air, ASME, Glasgow, UK, pp. GT2010-22154.

[4] Harp, J. L., and Oatway, T. P., 1979, "Centrifugal Compressor Development for a Variable Area Turbocharger," SAE Technical Paper, pp. 790066.

[5] Wöhr, M., Müller, M., and Leweux, J., 2017, "Variable Geometry Compressors for Heavy Duty Truck Engine Turbochargers," ASME Turbo Expo 2017: Turbomachinery Technical Conference and Exposition, ASME, North Carolina, USA, pp. V008T26A015.

[6] Tange, H., Ikeya, N., Takanashi, M., and Hokari, T., 2003, "Variable Geometry Diffuser of Turbocharger Compressor for Passenger Vehicles," SAE 2003 World Congress & Exhibition, SAE International, USA, pp. 2003-01-0051.

[7] Czapka, T., Hagelstein, D., Theobald, J., Demmelbauer-Ebner, W., and Seume, J., 2016, "Turbocharger Compressor Map Enhancement for Highly Efficient Combustion Engines," 12th International Conference on Turbochargers and Turbocharging, IMechE, London, UK, pp. 15-31.

[8] Sun, Z., Tan, C., and Zhang, D., 2009, "Flow Field Structures of the Impeller Backside Cavity and Its Influences on the Centrifugal Compressor," ASME Turbo Expo 2009: Power for Land, Sea and Air, ASME, Florida, USA, pp. 1349-1360.

[9] Fischer, T., Rätz, H., Peters, M., and Seume, J., 2016, "Low Inertia Centrifugal Compressor Wheels: Influence of Back Disk Cavity on Aerodynamic Losses and Axial Thrust Load," 12th International Conference on Turbochargers and Turbocharging, IMechE, London, UK, pp. 303-317.

[10] Kaluza, P., Landgraf, C., Schwarz, P., Jeschke, P., and Smythe, C., 2017, "On the Influence of a Hubside Exducer Cavity and Bleed Air in a Close-Coupled Centrifugal Compressor Stage," Journal of Turbomachinery, **139**(7).

[11] Tamaki, H., Nakao, H., and Saito, M., 1999, "The Experimental Study of Matching between Centrifugal Compressor Impeller and Diffuser," Journal of Turbomachinery, **121**(1), pp. 113-118.

[12] Runstadler, P.W., Dolan, F.X., and Dean, R.C., 1975, "Diffuser Data Book," Creare Inc., Hanover, N.H.

[13] Ziegler, K. U., Gallus, H. E., and Niehuis, R., 2003, "A Study on Impeller-Diffuser Interaction—Part I: Influence on the Performance," Journal of Turbomachinery, **125**(1), pp. 173-182.

[14] Ziegler, K. U., Gallus, H. E., and Niehuis, R., 2003, "A Study on Impeller-Diffuser Interaction—Part II: Detailed Flow Analysis," Journal of Turbomachinery, **125**(1), pp. 183-192.

[15] Van den Braembussche, R. A., 2014, "Centrifugal Compressor Analysis & Design," VKI Course Note 192, Brussels, Belgium.

[16] Cumpsty, N.A., 2004, "Compressor Aerodynamics," Krieger Publishing Company, Florida, USA.

[17] Tamaki, H., Unno, M., Kawakubo, T., and Hirata, Y., 2010, "Aerodynamic Design of Centrifugal Compressor for AT14 Turbocharger," IHI Engineering Review, **43**(2), pp. 70-76.

[18] Gibson, L., Galloway, L., Kim, S., and Spence, S., 2017, "Assessment of Turbulence Model Predictions for a Centrifugal Compressor Simulation," Journal of the Global Power and Propulsion Society, **1**(1), pp. 142-156.

[19] Japikse, D., 1996, "Centrifugal Compressor Design and Performance," Concepts NREC, White River Junction, VT.

[20] Harley, P., Spence, S., Filsinger, D., Dietrich, M., and Early, J., 2014, "Meanline Modeling of Inlet Recirculation in Automotive Turbocharger Centrifugal Compressors," Journal of Turbomachinery, **137**(1).

[21] Stuart, C., Spence, S., Filsinger, D., Starke, A., and Kim, S., 2017, "Characterizing the Influence of Impeller Exit Recirculation on Centrifugal Compressor Work Input," Journal of Turbomachinery, **140**(1).